

# Composites for Lightweight Structures

## Part A

### 1. Free-Body Diagram and Tip Deflection Prediction

#### 1.1 Free-Body Diagram and Shear and Bending Moment Diagram

The cantilevered wing substructure was analysed under the limit load with a shear stress of 9.8MPa applied at the at  $45^\circ$  in the xy-plane over the tip rib. The perimeter of the root is fully restrained. The wing was modelled as a cantilever beam with a span  $L=130\text{mm}$ . The tip rib's cross section was found to be  $324+9\pi\text{ mm}^2$  which yields  $F=3452.29\text{N}$ . The free-body diagram shows the wing with  $F$  as the applied force where  $x=0$  at the root and  $x=L$  at the tip.

$$V_x = V_y = -F_{x,y} = -2441.14\text{N} \quad (1)$$

$$M(x) = (F_x)(L - x) = 317348.2\text{Nm} \quad (2)$$

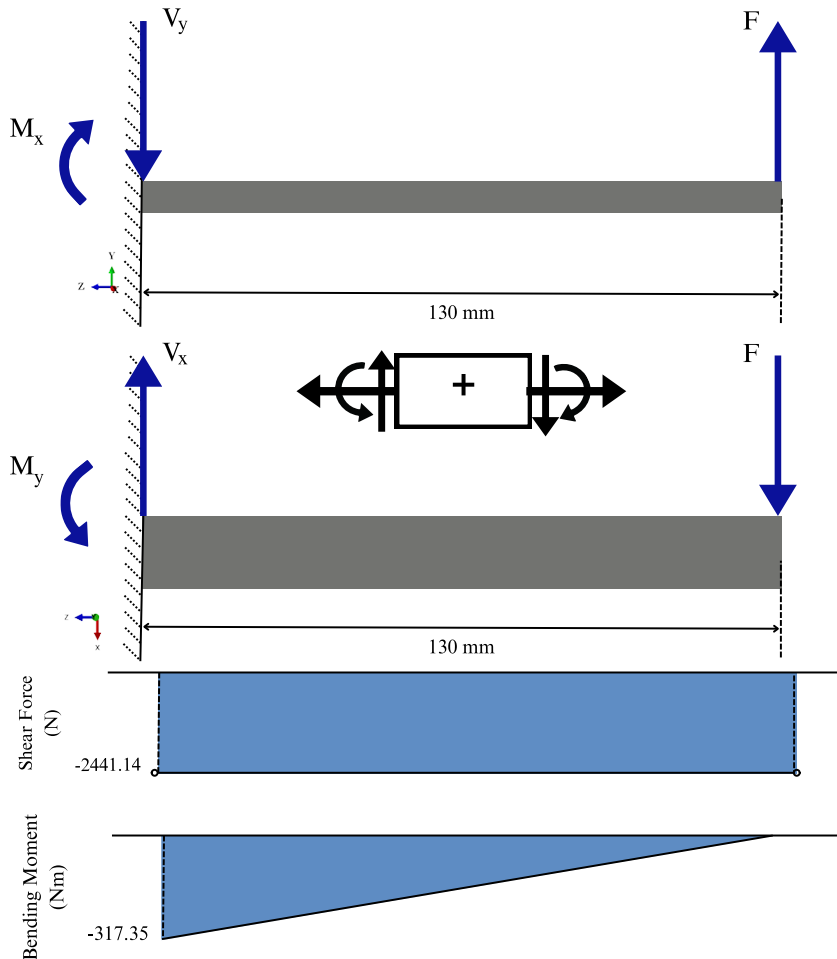


**Figure 1:** Free-Body Diagram, Shear and Bending Moment Distribution over Span.

#### 1.2 Analytical Prediction of Tip Deflection

To find the tip deflections using Euler-Bernoulli beam theory, the second moment of area of the cross section ( $I_{xx}$  and  $I_{yy}$ ) was required. The cross section is symmetric about the x-axis and shown in the Figure 2. It was discretised into rectangular sections and curved edges with the thickness of the laminate considered. The  $E_{eff}$  was found to be 54.1GPa which was found using the given quasi-isotropic laminate by Composite Laminate Theory.

### 3.3 Nonlinear Onset of First Instability

A geometric nonlinear analysis was performed using the Riks method with the NLGEOM option enabled to predict the buckling onset under the limit load. The Riks method was chosen to capture the buckling and post-buckling behaviour by tracking the load proportionality factor (LPF) and the magnitude of the displacement (U). To initiate the analysis an imperfection of 0.001mm was introduced based on the linear buckling mode shape from Section 3.2. This was introduced to make the structure more susceptible to local instability as without it the structure is perfect and may lead to exhibit unrealistically high buckling resistance. The displacement was monitored at the node which had the maximum deformation in the linear buckling analysis to ensure that we track the buckling response accurately.

The LPF vs U plot is shown in Figure 3(b) and shows that it exhibits a nonlinear response. The curve rises linearly to around an LPF of 0.4 with a maximum displacement of less than 0.1mm and then exhibits a slope change at LPF = 0.438, indicating buckling at 4.29MPa. Post buckling the structure can carry more load with LPF increasing linearly from 0.8 to 1.6. The two points marked in Figure 3 are where buckling starts and then stabilises. The structure snaps from that point to the next. Compared to the linear and analytical prediction the nonlinear critical load at 4.29MPa is 60% lower. The linear analysis overestimates stability by assuming perfect geometry and elasticity while the analytical assumes a simply supported plate under uniaxial compression. The Riks method, the most accurate prediction, which includes geometric nonlinearity and imperfections trigger early buckling showing that the structure is susceptible to compressive stresses. In addition, it is more accurate cause it is validated by the post buckling agreement with the design requirements, so it is the more reliable estimate.

## 4. Design Criteria Evaluation

### 4.1 Contour Plots of Displacements and Strains

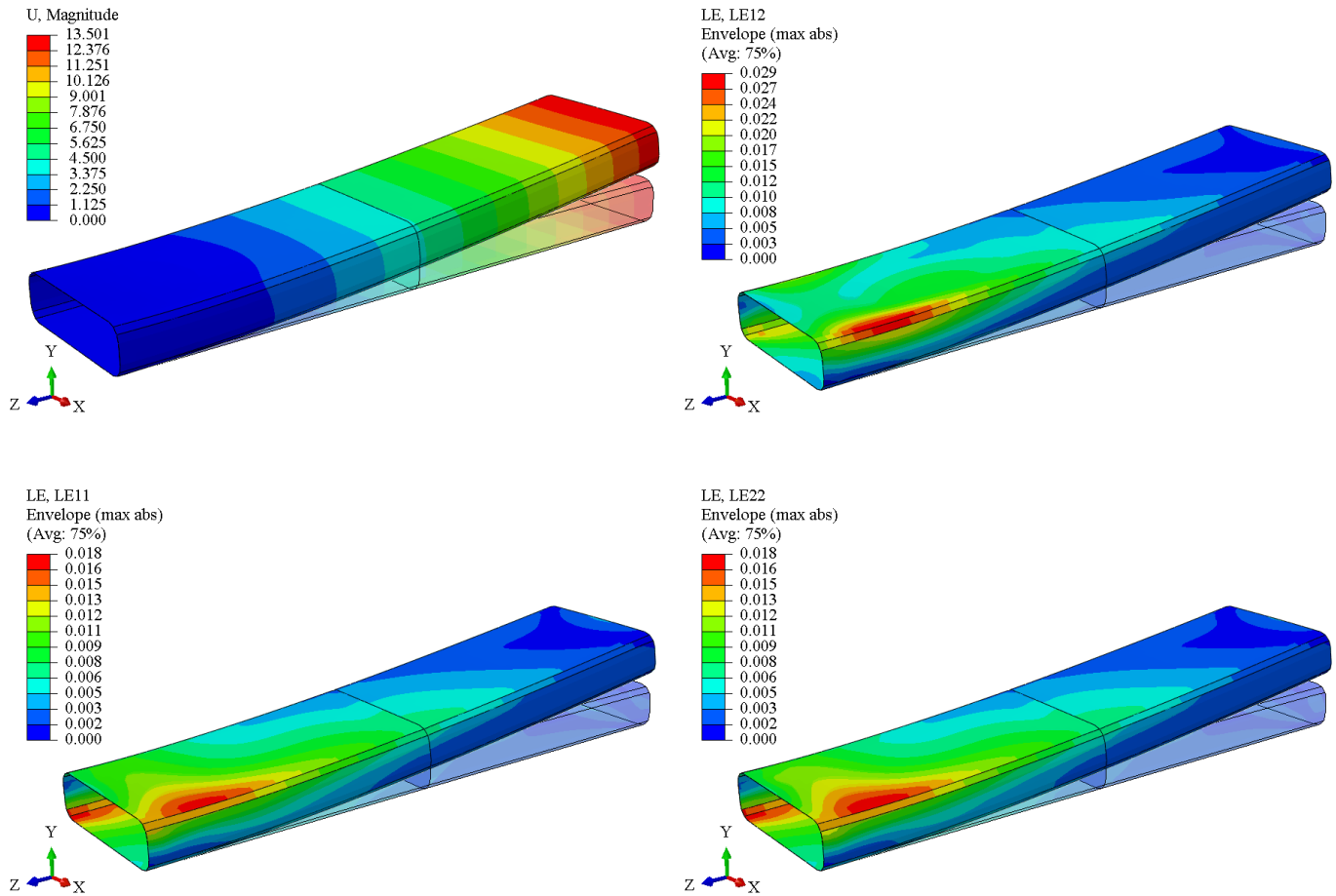


**Figure 4:** (a) Displacement at the limit load (b) Shear strain (c) Longitudinal Strain (d) Transverse Strain.

Contour plots of displacements and strains were generated from the nonlinear analysis conducted in the section above. Figure 4(a) shows the tip deflections and reveal a gradient of deformation with a max displacement at the tip and near zero near the root. The strain contour plots highlight the longitudinal strain (LE11), transverse strain (LE22) and the shear strain (LE12) where it peaks at 0.018, 0.018 and 0.029 respectively. LE11 and LE22 peaks at the root cover and the bottom of the curved root spar on the far side. LE12 peaks at the top of the root spar on the near side. The 0° plies in the root layup resist longitudinal deformation, constraining U1, while the 45° load amplifies U2 through shear-bending coupling. The LE12 peak (0.029) at the root spar's top (near side) aligns with the ±45° plies' shear resistance under the 45° load. The results' accuracy relies on mesh refinement, which appears sufficient given smooth gradients, though finer elements could refine strain peaks.

#### 4.2 Failure Load and Tip Deflection at Limit Load

**Table 2:** Hashin's Failure Criteria

Ply	Angle	HSNFCCRT F= 7.081 MPa	HSNFTCRT F= 9.781 MPa	HSNMCCRT F= 8.749 MPa	HSNMTCRT F= 7.081 MPa
1	-45°	0.2380	0.2620	0.3890	1.0400
2	+45°	0.4920	0.3220	0.3380	0.9560
3	90°	0.0981	0.1480	0.0458	1.0500
4	0°	1.0600	1.0100	0.1090	0.0904
5	-45°	0.2150	0.2360	0.2530	1.0500
6	+45°	0.4420	0.3340	0.3270	0.9230
7	90°	0.0977	0.0499	0.0396	1.0300
8	0°	1.0400	0.9990	0.0649	0.0945
9	0°	1.0300	0.9970	0.0618	0.0956
10	90°	0.0974	0.8080	0.0530	1.0200
11	-45°	0.3830	0.3500	0.4680	0.0883
12	+45°	0.1770	0.1940	0.6360	1.0500
13	0°	1.0000	0.9890	0.0419	0.1010
14	90°	0.1030	0.2660	0.0458	1.0100
15	-45°	0.3410	0.3630	0.8730	0.0872
16	+45°	0.1830	0.1720	1.0900	1.0500
<b><math>\delta_x</math> (Horizontal)</b>		1.348 mm	1.904 mm	1.683 mm	1.348 mm
<b><math>\delta_y</math> (Vertical)</b>		9.112 mm	13.4 mm	11.56 mm	9.112 mm

The structure first fails at 7.08MPa due to fibre compression. The primary failure mode is fibre compression in 0° plies and matrix tension at -45° and 90° in the upper level of the midplane and +45° and 90° at the lower level of the midplane. The matrix tension failure occurs at the bottom left spar near the root and the fibre compression at the top right root cover. Table 2 summarises the Hashin indices for all the plies at their critical load showing where the first plies fail and their respective deflections. At 9.8MPa indices increase further indicating progressive damage.

The wingbox undergoes bending because the 0°plies are responsible for carrying the axial loads and because of the applied shear load causing compressive stresses on the upper skin and tensile stresses at the bottom skin. For fibre tension, the 0° plies failed for the same reason.

The matrix compression failure in the +45 ply of the bottom skin is due to the combined shear and transverse compression. The ±45° plies carry shear loads, which generate transverse tensile stresses in the matrix. As the shear load increases, the matrix tensile strength is exceeded, resulting in micro-cracking and eventual failure. Figure 5 shows the most critical regions of failure according to Hashin's criteria.

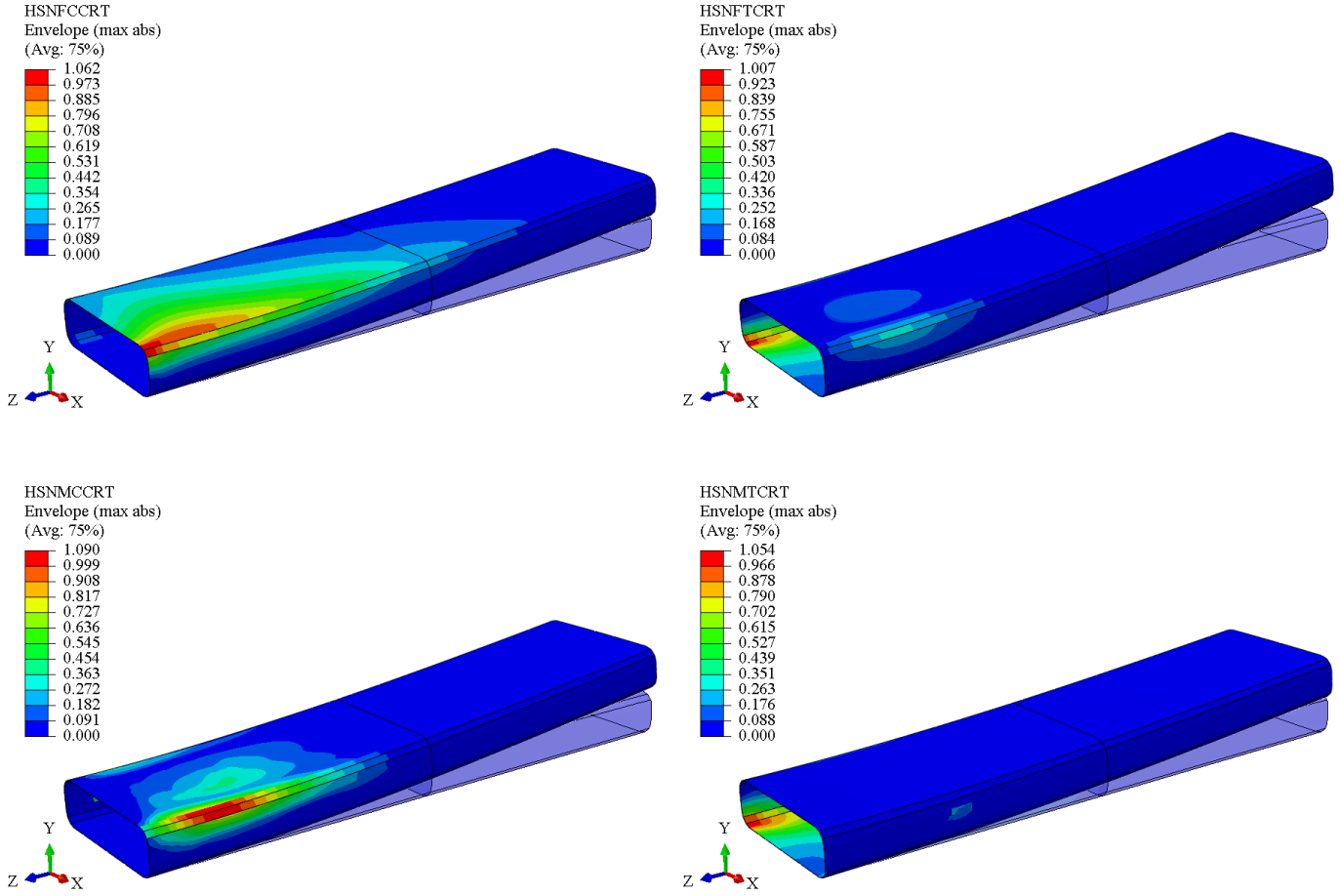


**Figure 5:** Contour plots for Hashin Criteria at different critical loads.

The contour plots show that failure initiates in two primary regions which are consistent with the high strains observed in Section 4.1. Fibre compressive failure near the root aligns where the longitudinal and transverse strain is peak, as this is due to the bending stresses. Matrix tension failure occurs at the top of the root spar and corresponds to the shear strain showing that matrix cracking has initiated due to shear and transverse tension in those failed plies.

### 4.3 Compliance with Design Constraints

Table 3 outlines the design constraints and assesses the compliance of the current design. This design requires optimisation to reduce the vertical tip deflection and increase the failure load to 9.8MPa while maintain compliance with the other criteria.

**Table 3:** Evaluation of Design Constraints

Criteria	Required Values	Actual Value	Satisfied
Vertical Tip Deflection	$\leq 12$ mm	13.372 mm	No
Horizontal Tip Deflection	$\leq 2$ mm	1.904 mm	Yes
Material Damage	Not Allowed	Failure at 7.08MPa (Hashin)	No
Buckling Stability	Tolerated	Buckling at 4.29MPa, stable to 9.8MPa	Yes
Maximum Mass	$\leq 31.75$ g	30.63 g	Yes
Laminate Constraints	Balanced and Symmetric		

## 5. Design Optimization

To mitigate the design deficiencies identified above the substructure was optimized by modifying the laminate layup configuration. Due to the symmetry, only half of the new sequence is provided in Table 5, while the full stacking sequence is shown in Figure 6.